I&EC research
Industrial & Engineering Chemistry Research

pubs.acs.org/IECR

Article

Process Modeling of CO_2 Absorption with Monoethanolamine Aqueous Solutions Using Rotating Packed Beds

Cheng-Hsiu Yu, Yu-Jeng Lin, David Shan-Hill Wong, and Chau-Chyun Chen*

Cite This: *Ind. Eng. Chem. Res.* 2022, 61, 12142−12152

Read Online

ACCESS | Metrics & More | Article Recommendations

ABSTRACT: A first-principle process simulation model is presented for the chemical absorption of carbon dioxide (CO_2) with monoethanolamine (MEA) aqueous solutions using rotating packed beds (RPB). Built on a proven rate-based packed bed absorber model, the RPB model rigorously simulates the phase and chemical equilibria at the vapor−liquid interface, the heat and mass transfer across the gas and liquid films, the fast reactions between MEA and CO_2 in the liquid film, and the RPB hydraulics. Estimation of the rate of transfer of mass across the liquid film is central to accurate simulation of the CO_2 absorption process with MEA aqueous solutions. We show that the literature lab-scale RPB data for CO_2 removal efficiency can be satisfactorily correlated by introducing a correction factor for the effective packing surface area predicted by the Onda correlation. Given the validated RPB model, we further show that, among the gas-phase mass transfer coefficient, the liquid-phase mass transfer coefficient, and the reaction rate constant for the reaction between amine and CO_2, the reaction rate constant is the controlling step with the greatest potential to enhance the CO_2 absorption performance in RPB.

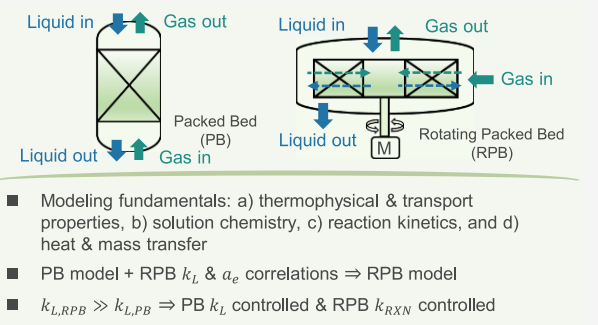

1. INTRODUCTION

Carbon dioxide (CO_2) capture with chemical absorption is the most mature process technology for reducing the emissions of CO_2 from fossil fuel-fired power plants.[1] Conventional CO_2 chemical absorption processes with packed beds (PB) require excessive packing volume in the CO_2 absorber due to the large mass transfer resistance across the gas−liquid interface.[2] As a process intensification alternative to PB, rotating packed beds (RPB) have been experimentally investigated by many researchers for their use in CO_2 capture with chemical absorption.[3−10] Moreover, extensive process simulation efforts for CO_2 capture with RPB have been reported to capture process fundamentals of CO_2 chemical absorption and to predict CO_2 removal efficiency.[4,11−15]

Prior works in modeling CO_2 chemical absorption with monoethanolamine (MEA) aqueous solutions in RPB applied either the enhancement-factor approach[4,11,14,15] or the rate-based approach.[12,13] The enhancement factor is defined as the ratio of the effective liquid mass transfer coefficient for absorption with and without chemical reaction and is typically estimated with an approximated concentration profile in the liquid film. Despite satisfactory agreements with lab-scale data[4,6] and pilot-scale data,[3] these prior studies suffer from several common issues in the model formulation: (1) estimation of the reaction rate based on species concentration,[4,11,14,15] (2) reaction speciation expressed in terms of apparent components,[4,15] (3) use of the incorrect liquid volume in estimating the reaction rate in the film,[4,11] (4) failure to consider energy balance,[4] and (5) questionable estimation of the superficial liquid velocity.[11]

In contrast to the enhancement-factor approach, the rate-based approach assumes the equilibrium is achieved only at the gas−liquid interface, the Maxwell−Stefan theory is used to calculate the multicomponent mass transfer, and the CO_2 absorption depends on the finite mass transfer rates in contacting phases and the reaction rates in the liquid film estimated with explicit concentration profiles for each discretized liquid film segment. For systems involving fast reaction rates that have finite CO_2 mass transfer, i.e., CO_2 chemical absorption with MEA aqueous solutions, the rate-based approach is appropriate for capturing the changing concentration gradients in the gas and liquid films with two-film theory and to provide precise calculations. Prior modeling studies with the rate-based approach have successfully described the pilot-scale RPB data.[12,13] However, improvements are desirable for addressing several modeling deficien-

Special Issue: In Honor of Joan F. Brennecke

Received: November 1, 2021
Revised: January 16, 2022
Accepted: January 26, 2022
Published: February 9, 2022

cies: (1) assumption of a constant bed diameter for each gas−liquid contacting section in RPB, (2) estimation of the reaction rate based on species concentration, and (3) no indication of whether film discretization was considered.

Yu et al.[4] simulated CO_2 absorption in RPB with a 30 wt % unloaded MEA aqueous solution. Adopting the enhancement-factor approach, they presented a simplified RPB model with the pseudo-first-order reaction rate expression developed by Hikita.[16] They applied the Onda correlations[17] for the estimation of effective packing surface area a_e and gas-phase mass transfer coefficient k_G and the Tung and Mah correlation[18] for liquid-phase mass transfer coefficient k_L. The total RPB packing volume was treated as the reaction volume, and hence, no liquid holdup correlation was needed in the simplified model. Although their modeling results showed good agreement with data,[4] their RPB model considered neither the electrolyte solution chemistry nor the energy balance.

Kang et al.[11] modeled CO_2 absorption with MEA aqueous solutions in RPB for process scale-up. The enhancement-factor approach was utilized with the reaction rate expression and parameters taken from Aboudheir et al.[19] and the liquid-phase nonideality accounted for with the electrolyte nonrandom two-liquid (eNRTL) activity coefficient model.[20] After examining various combinations of hydraulics correlations, they showed the RPB model predicted well the lab-scale data[4] and the pilot-scale data[3] with the Onda correlations[17] for a_e and k_G, the Tung and Mah correlation[18] for k_L, and the Burns correlation[21] for liquid holdup ε_L. Later, the RPB model was implemented by Thiels et al.[6] in Aspen Custom Modeler to validate against their lab-scale RPB data, which covered wide ranges of CO_2 lean loadings and gas flow rates. While the model satisfactorily predicted the data, it estimated the rate of reaction between MEA and CO_2 using the bulk liquid holdup and arbitrarily calculated the liquid molar flow rate from the liquid holdup, leading to questionable k_L and a_e.

Oko et al.[14] investigated the effect of intercooling in RPB for CO_2 absorption with a concentrated MEA solution (∼40−80 wt %). Applying the enhancement-factor approach, they used the reaction rate expression and parameters of Aboudheir et al.[19] and the eNRTL model for the liquid-phase nonideality. The hydraulics correlations included the Billet and Schultes correlation[22] for a_e, the Chen correlation[23] for k_G, and the Tung and Mah correlation[18] for k_L. The liquid holdup correlation was not specified. Calculating the reaction rate on the basis of species concentrations, the model predicted well the CO_2 removal efficiency.

Borhani et al.[15] examined eight reaction kinetic models and five enhancement-factor models for CO_2 absorption with MEA solutions in RPB. They applied the Wilson model for solution nonideality, the Onda correlations[17] for a_e and k_G, the Tung and Mah correlation[18] for k_L, and the Burns correlation[21] for ε_L. They showed that the reaction kinetic model of Luo et al.[24] with the enhancement-factor model developed by Wellek et al.[25] yields the best prediction for the CO_2 removal efficiency. Although their model satisfactorily predicted the pilot-scale RPB data,[3] their model estimated the reaction rate from the concentrations of the apparent species in the solution.

Joel et al.[12] applied the rate-based PB model in Aspen Plus to examine the effect of operational variables on the CO_2 removal efficiency for a pilot-scale RPB. They observed no temperature bulges for the concentrated MEA solutions (55 and 75 wt %) within the RPB due to the high solvent:gas ratio (∼30 kg/kg). They defined the height of the PB as the difference between the inner and outer radii of the RPB. The diameter of the PB was determined to yield the same volume as that of the RPB. The eNRTL model was applied to account for the liquid-phase nonideality. The concentration-based reaction rate expression and the model parameters were retrieved from *Aspen Properties*.[26] The hydraulics correlations included the Onda correlations[17] for a_e and k_G, the Tung and Mah correlation[18] for k_L, and the Burns correlation[21] for ε_L. While the model predictions satisfactorily represented the pilot-scale RPB data, in a subsequent study[13] they further examined the applicability of other hydraulics correlations, including the Luo12 correlation[27] for a_e, the Chen correlation[23] for k_G, the Chen correlation[28] for k_L, and the Burns correlation[21] for ε_L. They reported the improved predictions compared to the correlations adopted by Joel et al.[12] However, these two studies assumed a constant bed diameter for all gas−liquid contacting sections and did not report whether film discretization was considered in the rate-based PB model.

This study aims to develop a first-principle RPB process simulation model for CO_2 chemical absorption with MEA aqueous solutions. Addressing the deficiencies of prior studies, the RPB model adopts the rate-based approach to estimate the heat and mass transfer across the discretized liquid film, calculates the phase equilibrium at the vapor−liquid interface on the basis of a proven thermodynamic model,[29] estimates the reaction rate with a validated activity-based kinetic model,[29,30] and accounts for the changing bed diameters and the corresponding gravitational field for gas−liquid contacting sections in RPB.

2. MODEL FORMULATION

The rate-based packed bed column model in Aspen Plus V10[31] is used as the foundational model to develop the RPB model because it offers a fully validated rigorous rate-based simulation framework for CO_2 chemical absorption in PB.[32−34] We hypothesize that the modeling fundamentals of PB and RPB are identical except for the gravitational field and the RPB geometry, which affect the hydraulics and therefore the CO_2 removal efficiency. Otherwise, CO_2 absorption in PB and RPB should share identical modeling fundamentals in terms of thermophysical and transport properties, solution chemistry, reaction kinetics, and heat and mass transfer. To capture the effect of the gravitational field on hydraulics in RPB, various hydraulic correlations will be examined to demonstrate their applicability for RPB. In addition, the RPB geometry will be properly accounted for within the framework of the rate-based PB model in Aspen Plus. To allow for precise calculation of reaction rates in the liquid film, the liquid film is discretized with five segments, as suggested by Zhang et al.[33] We further assume the mixed flow model for both the gas phase and the liquid phase in each PB segment. In other words, the bulk properties of the gas phase and the liquid phase are assumed to be the same as the outlet conditions of the phases leaving the segment.

2.1. Thermophysical and Transport Properties. The solution chemistry involved in the absorption of CO_2 with MEA aqueous solutions includes water dissociation, CO_2 hydrolysis, bicarbonate dissociation, carbamate hydrolysis, and MEA protonation. They are shown as eqs 1−5:

$$2H_2O \leftrightarrow H_3O^+ + OH^- \quad (1)$$

https://doi.org/10.1021/acs.iecr.1c04323
Ind. Eng. Chem. Res. 2022, 61, 12142−12152

$$CO_2 + 2H_2O \leftrightarrow H_3O^+ + HCO_3^- \quad (2)$$

$$HCO_3^- + H_2O \leftrightarrow H_3O^+ + CO_3^{2-} \quad (3)$$

$$MEACOO^- + H_2O \leftrightarrow MEA + HCO_3^- \quad (4)$$

$$MEA + H_3O^+ \leftrightarrow MEAH^+ + H_2O \quad (5)$$

The thermodynamic model developed by Zhang et al.[29] for the $MEA/CO_2/H_2O$ system is chosen to model the system. Specifically, the eNRTL model and perturbed-chain statistical associating fluid theory (PC-SAFT) equation of state[35] are applied to account for the liquid-phase and gas-phase nonidealities, respectively. This thermodynamic model has been validated and can well represent the vapor−liquid equilibrium, heat capacity, excess enthalpy, and speciation data for the $MEA/CO_2/H_2O$ system over a wide range of temperatures, pressures, MEA concentrations, and CO_2 loadings.[29]

The transport properties of interest include density, viscosity, surface tension, thermal conductivity, and diffusivity. The work incorporates the correlation developed by Weiland et al.[36] for the viscosity of MEA aqueous solutions. The other transport properties are calculated with the empirical transport property methods available in Aspen Plus.[31]

2.2. Reaction Kinetics. The reaction kinetics are expressed in terms of the carbamate formation reaction and bicarbonate formation reaction shown in eqs 6 and 7, respectively. The forward and reverse reaction rate expressions with activity basis are given in eqs 8−11.

$$2MEA + CO_2 \leftrightarrow MEAH^+ + MEACOO^- \quad (6)$$

$$MEA + CO_2 + H_2O \leftrightarrow MEAH^+ + HCO_3^- \quad (7)$$

$$r^f_{MEACOO^-} = k^f_{MEACOO^-} a_{MEA}{}^2 a_{CO_2} \quad (8)$$

$$r^r_{MEACOO^-} = k^r_{MEACOO^-} a_{MEAH^+} a_{MEACOO^-} \quad (9)$$

$$r^f_{HCO_3^-} = k^f_{HCO_3^-} a_{MEA} a_{CO_2} \quad (10)$$

$$r^r_{HCO_3^-} = k^r_{HCO_3^-} \frac{a_{MEAH^+} a_{HCO_3^-}}{a_{H_2O}} \quad (11)$$

The temperature-dependent expression for the reaction rate constants is given in eq 12. As shown in Table 1, the reaction rate constants for the carbamate formation reaction and the bicarbonate formation reaction were retrieved from Plaza,[30] who reported that the deviation between the experimental and calculated CO_2 absorption rate is ±20% for a 30 wt % MEA solution with the loading range of 0.15−0.45 mol of CO_2/mol of MEA.

Table 1. Reaction Kinetic Constants for Carbamate and Bicarbonate Formation of the MEA/CO_2 System[30]

reaction	reaction direction	k_j^o (kmol m^{-3} s^{-1})	E_j (kJ mol^{-1})
carbamate formation	forward	8.56×10^{10}	3.96
	reverse	24800	59.60
bicarbonate formation	forward	22991.13	49.00
	reverse	18.35	96.23

$$k_j = k_j^o \exp\left[-\frac{E_j}{R}\left(\frac{1}{T} - \frac{1}{298.15}\right)\right] \quad (12)$$

2.3. Hydraulics Correlations. The hydraulics correlations considered in this work are summarized in Table 2. The Onda correlations[17] (eqs 13 and 14) are used to estimate k_G and a_e. Although the Onda correlations were developed for PB, prior RPB modeling studies[4,11,12,15] predicted CO_2 removal efficiency satisfactorily with the Onda correlations. Derived from penetration theory for RPB, the Tung and Mah correlation[18] (eq 15) is used to estimate k_L. It is worth noting that Tung and Mah suggested that "liquid mixing at the junctions of packing materials may be more complete in Higee process than in traditional process" and the liquid-phase mass transfer coefficients in RPB would be 4−10 times higher than those in conventional PB. The Burns correlation[21] (eq 16) that was developed specifically for RPB is used to estimate ε_L. Prior RPB modeling studies[11−13,15] have shown satisfactory results with the Burns correlation.

The heat transfer coefficient h is estimated by the Chilton and Colburn analogy method[37] from the binary mass transfer coefficient. The method was developed on the basis of the assumption that the mechanisms of mass transfer and heat transfer are similar and analogous to each other. Specifically, h is estimated using the physical and transport properties of the vapor or liquid phase, such as the average mass transfer coefficient, molar density, thermal conductivity, and specific molar heat capacity, as shown in eq 17.

Note that we also examined the applicability of two additional a_e correlations developed specifically for RPB: the Luo12 correlation (eq 18)[27] and the Luo17 correlation (eq 19).[38]

The gravitational field increases along the radial direction in RPB at a fixed rotating speed. We implemented customized user subroutines for the hydraulics correlations in Aspen Plus to calculate the centrifugal acceleration, g_c, from the mean radius of each RPB section and the square of the rotating speed.

3. LAB-SCALE DATA AND DATA RECONCILIATION

The lab-scale RPB experimental data reported by Thiels et al.[6] are used to validate the RPB model developed in this work. The specifications and operational conditions of the experimental RPB are summarized in Table 3. The inner diameter, outer diameter, and height of the experimental RPB were 0.025, 0.125, and 0.023 m, respectively. Stainless steel wire mesh was used as the packing, where the specific surface area and the void fraction were 887.6 m^2/m^3 and 0.96, respectively. A 30 wt % MEA solution was used to absorb 10% CO_2 from nitrogen in the gas stream in RPB. Without reporting the uncertainty of the data, Thiels et al.[6] reported the CO_2 removal efficiency as a function of the gas flow rate and the lean loading. The gas flow rate ranged from 5 to 60 L/min, while the liquid flow rate was fixed at 0.1 L/min. The 30 wt % MEA solution was fed into the RPB at five lean loadings, ranging from 0 to 0.442 mol of CO_2/mol of MEA. The inlet temperatures of the gas and liquid flows were controlled at 323 K. The rotating speed was fixed at 1600 rpm. Given the experimental rotating speed, the estimated gravitational field was in the range of 36−179 g from the inner to outer radii of RPB.

Figure 1 illustrates the schematic diagram for the RPB and its representation as a PB in Aspen Plus. The RPB in the radial

https://doi.org/10.1021/acs.iecr.1c04323
Ind. Eng. Chem. Res. 2022, 61, 12142−12152

Table 2. Hydraulics Correlations Applied in the RPB Model

source	correlation type	expression
Onda correlation[17]	k_G	$\frac{k_G RT}{a_t D_G} = 2.0 Re_G^{0.7} Sc_G^{1/3} (a_t d_p)^{-2.0}$ (13)
	a_e	$\frac{a_e}{a_t} = 1 - \exp\left[-1.45\left(\frac{\sigma_c}{\sigma_L}\right)^{0.75} Re_L^{0.1} Fr_L^{-0.05} We_L^{0.2}\right]$ (14)
Tung and Mah correlation[18]	k_L	$\frac{k_L d_p}{D} = 0.92\left(\frac{a_t}{a_e}\right)^{1/3} Sc_L^{1/2} Re_L^{1/3} Gr_L^{1/6}$ (15)
Burns correlation[21]	ε_L	$\varepsilon_L = 0.039\left(\frac{g_c}{g_o}\right)^{-0.5}\left(\frac{U}{U_o}\right)^{0.6}\left(\frac{\nu}{\nu_o}\right)^{0.22}$ (16)
Chilton and Colburn method[37]	h	$h = \overline{k}\overline{\rho} c_p \left(\frac{\lambda}{\overline{\rho} c_p \overline{D}}\right)^{2/3}$ (17)
Luo12 correlation[27]	a_e	$\frac{a_e}{a_t} = 66510 Re'^{-1.41}_L Fr'^{-0.12}_L \varphi^{-0.74}$ (18)
Luo17 correlation[38]	a_e	$\frac{a_e}{a_t} = 15.17 Re'^{0.16}_G Re'^{-0.38}_L Fr'^{-0.13}_L We'^{0.45}_L \varphi^{-0.29}$ (19)

Table 3. RPB Specifications and Operational Conditions Reported by Thiels et al.[6]

Specifications	
diameter (m)	0.025 (inner), 0.125 (outer)
packing height (m)	0.023
packing volume ($\times 10^6$ m^3)	271
packing type	stainless steel wire mesh
porosity (−)	0.96
specific surface area (m^2/m^3)	887.6
Operational Conditions	
CO_2 inlet concentration (%)	10
gas flow rate (L/min)	5−60
gas inlet temperature (K)	323
MEA concentration (%)	30
liquid flow rate (L/min)	0.1
lean loading (mol of CO_2/mol of MEA)	0−0.442
liquid inlet temperature (K)	323
rotating speed (rpm)	1600

direction is divided into eight equally thick calculating segments. Each radial-direction segment in RPB is modeled as an axial-direction segment in PB. The specification of the rate-based PB model is shown in Table 4. Note that the height of the PB is the same as the thickness of the RPB, and for each segment, the diameter of the PB is calculated to yield the same bed volume as that of the RPB. As such, the cross-sectional area of the PB increases from the top to bottom segments.

The experimental data reported by Thiels et al.[6] for the CO_2 removal efficiency are reconciled by introducing an adjustable parameter called the interfacial area factor, a_e factor, to scale the predicted effective packing surface area in the RPB model. As we will discuss in more detail in Mass Transfer Studies, adjustments on k_G and k_L have little impact on the CO_2 removal efficiency for this liquid film controlling and high-reaction rate absorption process. The experimental uncertainties were estimated from the previously reported mass balance measurement and equipment error (e.g., the liquid pump, the

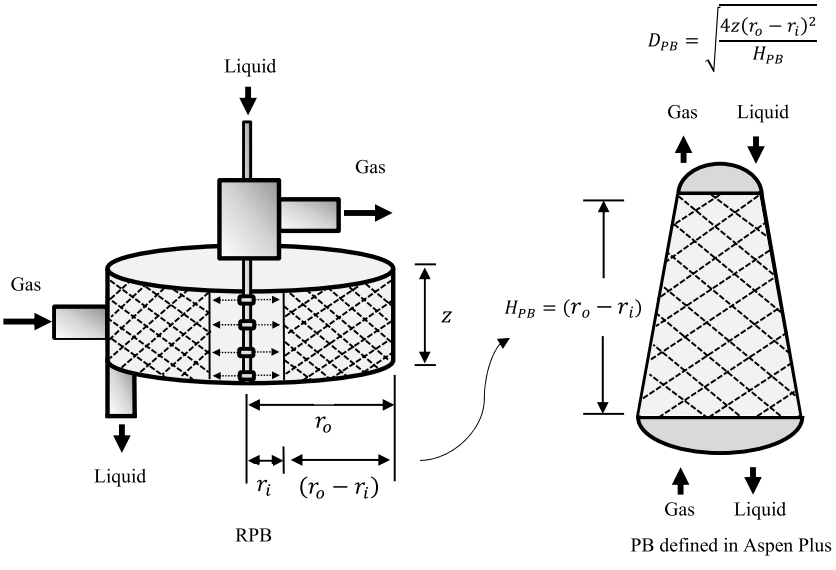

Figure 1. Schematic diagram of RPB and the corresponding PB defined in Aspen Plus.

https://doi.org/10.1021/acs.iecr.1c04323
Ind. Eng. Chem. Res. 2022, 61, 12142−12152

mass flow controller for gas, and the CO_2 concentration analyzer).[39] Table 5 shows the standard deviations assigned in the data reconciliation.

Table 4. Specifications of the Rate-Based PB Model for Modeling the RPB Data Reported by Thiels et al.[6]

packing type	coil
effective packing diameter (m)	0.00027
porosity (−)	0.96
specific surface area (m^2/m^3)	887.6
total height (m)	0.05
no. of sections	8
diameter of the sections (m)	0.05362−0.10452
volume for each section ($\times 10^6$ m^3)	14, 20, 25, 31, 37, 42, 48, 54

Table 5. Standard Deviations Assigned for Input and Output Variables

variable	standard deviation
liquid flow rate (mL/min)	1.0
loading (mol of CO_2/mol of MEA)	0.01
gas inlet flow rate (L/min)	0.48
CO_2 removal efficiency (%)	5

The objective function to be minimized for the data reconciliation is shown in eq 20:

$$\text{Obj} = \sum_{i=1}^{N_{sets}} \sum_{j=1}^{N_{exp}} \sum_{m=1}^{N_r} \left(\frac{X_{mr} - X_r}{s_{mr}} \right)^2 \quad (20)$$

The absolute relative deviation (ARD) is used to evaluate modeling results for CO_2 removal efficiency and is defined in eq 21:

$$\text{ARD}\,(\%) = \frac{1}{N_{exp}} \sum_{i=1}^{N_{exp}} \left| \frac{(C_i^{exp} - C_i^{cal})}{C_i^{exp}} \right| \times 100\% \quad (21)$$

4. MODELING RESULTS AND DISCUSSION

The modeling results of the base case RPB model are shown in Figure 2. The base case RPB model has no adjustable parameters, and the a_e factor is unity. The base case model predictions qualitatively match the observed experimental data trend on the CO_2 removal efficiency at various lean loadings and liquid:gas ratios, supporting the idea that the approach modeling RPB with the conventional rate-based PB model is appropriate. However, the base case model consistently overpredicts the removal efficiency due to the overpredictions of the Onda correlation for the effective packing surface area of the RPB wire mesh packing. The ARD between the experimental and predicted removal efficiencies is 28.5%. Subsequently, we adjusted the a_e factor to minimize the difference between the modeling results and the experimental removal efficiency. The modeling results with an a_e factor of 0.519 show satisfactory agreement with the data, and the ARD is reduced to 10.0%, as shown in Figure 2 and Table 6. At lean loadings of $\lesssim$0.16 mol of CO_2/mol of MEA, the removal efficiency decreases linearly with respect to the gas flow rate. At lean loadings of $\gtrsim$0.16 mol of CO_2/mol of MEA, the removal efficiency decreases rapidly and then decreases slowly with an increase in the gas flow rate, indicative of CO_2 saturation in the MEA solution.

Table 6. Identified a_e Factors for Various a_e Correlations and the Corresponding Absolute Relative Deviations

a_e correlation	a_e factor	ARD (%)
Onda correlation[17]	unity	28.5
Onda correlation[17]	0.519 ± 0.028	10.0
Luo12 correlation[27]	unity	56.8
Luo12 correlation[27]	0.185 ± 0.010	15.4
Luo17 correlation[38]	unity	53.8
Luo17 correlation[38]	0.213 ± 0.011	13.3

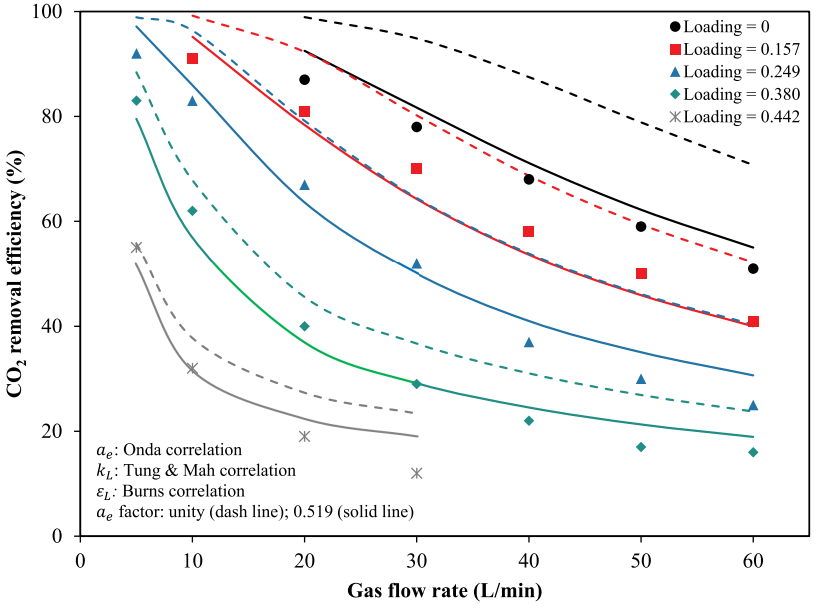

Figure 2. Modeling results with various lean loadings of 30 wt % MEA solutions. k_L is for the Tung and Mah correlation.[18] k_G and a_e are for the Onda correlations.[17] ε_L is for the Burns correlation.[21] Symbols represent experimental data for the CO_2 removal efficiency.[6] Dashed lines indicate the a_e factor for the Onda correlation[17] is unity (base case). Solid lines indicate the a_e factor for the Onda correlation is 0.519.

https://doi.org/10.1021/acs.iecr.1c04323
Ind. Eng. Chem. Res. 2022, 61, 12142−12152

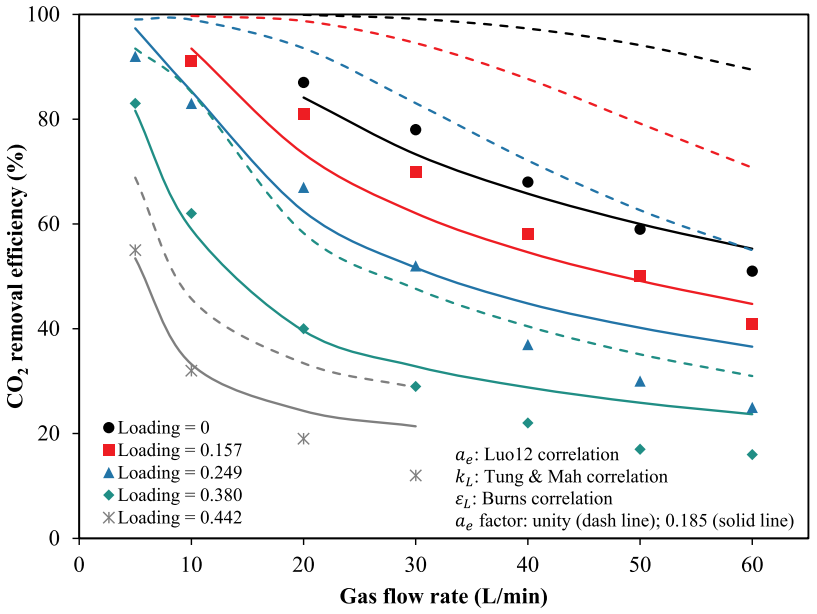

Figure 3. Modeling results with various lean loadings of 30 wt % MEA solutions. k_L is for the Tung and Mah correlation.[18] k_G is for the Onda correlation.[17] a_e is for the Luo12 correlation.[27] ε_L is for the Burns correlation.[21] Symbols represent experimental data for the CO_2 removal efficiency.[6] Dashed lines indicate the a_e factor for the Luo12 correlation is unity. Solid lines indicate the a_e factor for the Luo12 correlation is 0.185.

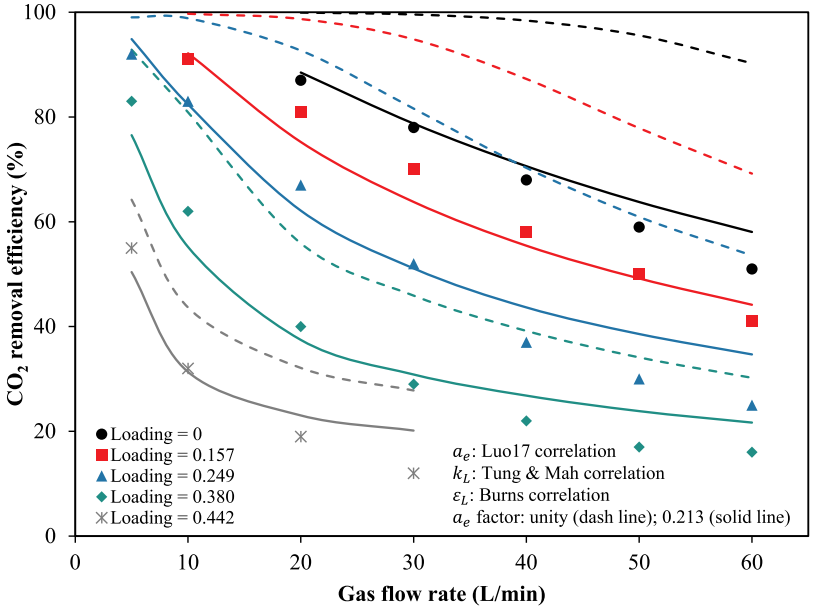

Figure 4. Modeling results with various lean loadings of 30 wt % MEA solutions. k_L is for the Tung and Mah correlation.[18] k_G is for the Onda correlation.[17] a_e is for the Luo17 correlation.[38] ε_L is for the Burns correlation.[21] Symbols represent experimental data for the CO_2 removal efficiency.[6] Dashed lines indicate the a_e factor for the Luo17 correlation is unity. Solid lines indicate the a_e factor for the Luo17 correlation is 0.213.

Figures 3 and 4 show the modeling results with the Onda correlation replaced with the Luo12[27] and Luo17[38] correlations for the effective packing surface area, respectively. The Luo12 correlation and the Luo17 correlation show no improvements over the Onda correlation for the CO_2 removal efficiency. The ARDs between the experimental and predicted removal efficiencies are 56.8% and 53.8% for the Luo12 and Lou17 correlations, respectively. To provide the best fittings to the data, the a_e factor was optimized to be 0.185 and 0.213 for Luo12 and Luo17, respectively. The corresponding ARDs are reduced to 15.4% for Luo12 and 13.3% for Luo17, as shown in Table 6. Although the Luo12 and Luo 17 correlations were developed for wire mesh packings in RPB, they show no improvement over the Onda correlation. We note that the geometry and specification of the RPB packings used in developing the Luo12 and Luo17 correlations are different from those investigated by Thiels et al.,[6] likely leading to a different liquid dispersion on the packing surface and therefore a different effective interfacial area for mass transfer. Because a_e has a significant effect on the CO_2 removal efficiency, more reliable a_e correlations that cover various types of packing geometries and a wide range of operational conditions are desirable.

https://doi.org/10.1021/acs.iecr.1c04323
Ind. Eng. Chem. Res. 2022, 61, 12142−12152

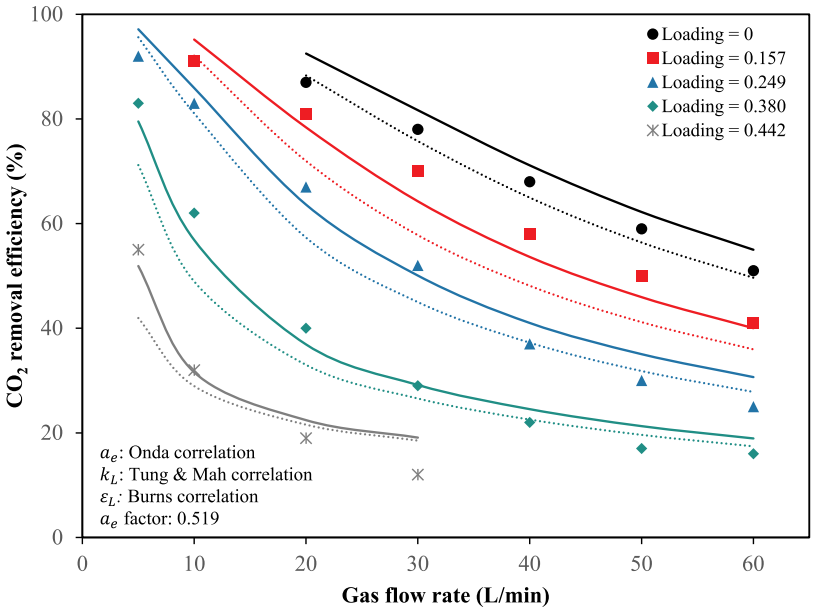

Figure 5. Effect of gravity on the CO_2 removal efficiency for the base case RPB model with an a_e factor of 0.519. Solid lines indicate the base case results, and dotted lines indicate unity gravity was assigned to the Onda correlation[17] for a_e.

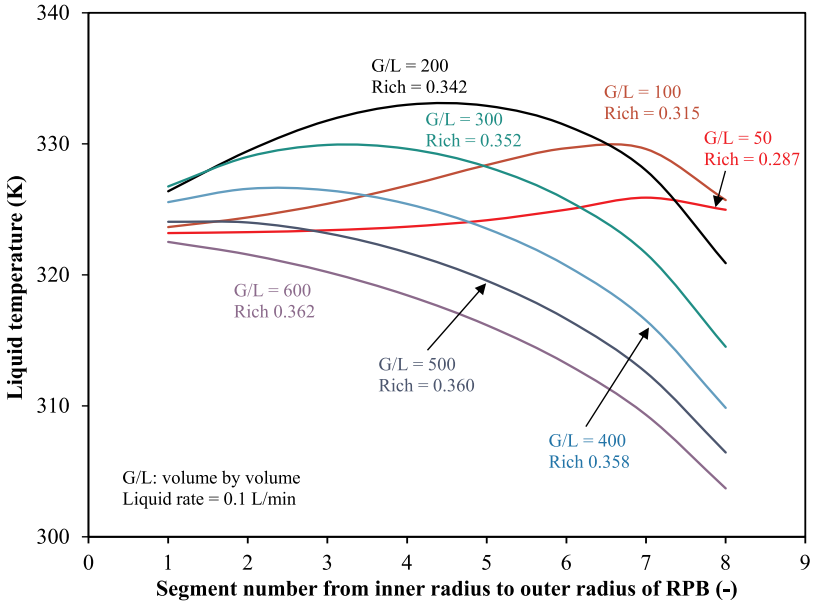

Figure 6. Temperature distribution across the RPB for the base case RPB model with an a_e factor of 0.519 at various gas:liquid flow rate ratios. The lean loading was 0.249 mol of CO_2/mol of MEA. The liquid rate was 0.1 L/min. The gas and liquid inlet temperatures were 323 K. The gas consisted of 10% CO_2 and 90% N_2.

We further examined the effects of k_L and ε_L on the CO_2 removal efficiency because the CO_2 chemical absorption is controlled by the liquid film. It is observed that an adjustment of ±20% in k_L does not affect the CO_2 removal efficiency of the base case RPB model with an a_e factor as 0.519, and the modeling results overlap with those presented in Figure 2. The increase in k_L should reduce the liquid film thickness and increase the rate of mass transfer between the gas and liquid phases. This observation suggests that k_L is not the controlling resistance in RPB, and the increase (or decrease) in k_L has little impact on the CO_2 removal efficiency in RPB.

The bulk liquid holdup ε_L is the amount of liquid retained in the packing, and it is used to determine the reaction rate in the bulk liquid. Because the reaction between MEA and CO_2 takes place primarily in the liquid film, adopting different bulk liquid holdup ε_L correlations in the RPB model does not affect the CO_2 removal efficiency.

To investigate the effect of gravity on the CO_2 removal efficiency in RPB, we simulated the base case RPB model with an a_e factor of 0.519 and imposed a hypothetical condition of unity gravity (i.e., g_c = 9.8 m/s^2) upon the hydraulics correlations. Figure 5 shows that with unity gravity imposed upon the Onda correction for a_e, the CO_2 removal efficiency decreases by ~10% due to the loss of additional effective interfacial area resulting from the gravity field. The CO_2 removal efficiency is nearly unchanged when unity gravity is further imposed upon the Tung and Mah correlation for k_L and

https://doi.org/10.1021/acs.iecr.1c04323
Ind. Eng. Chem. Res. 2022, 61, 12142−12152

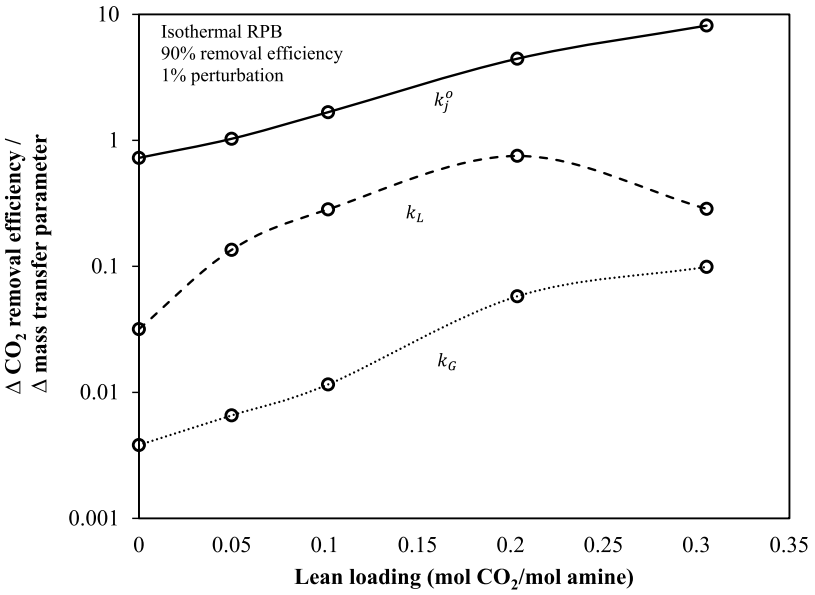

Figure 7. Contribution of mass transfer parameters k_L, k_G, and k_j^o to CO_2 removal efficiency at various lean loadings: temperature of 323 K, gas flow rate of 20 L/min, rotating speed of 1600 rpm, CO_2 removal efficiency of 90%, and effective area for mass transfer of 400 m^2/m^3 for each section.

the Burns correlation for ε_L as they are not the controlling factors of CO_2 absorption for RPB.

Figure 6 shows the temperature profiles of the gas and liquid in the base case RPB model with an a_e factor of 0.519 at a lean loading of 0.249 mol of CO_2/mol of MEA. The liquid and gas streams enter the RPB at 323 K from inside (segment 1) and outside (segment 8) of the RPB, respectively. Only the liquid temperature is presented as the gas temperature is nearly identical to the liquid temperature. As the gas:liquid (volume/volume) ratio increases from 50 to 200 (constant liquid flow rate of 0.1 L/min and varied gas rate), the temperature bulge moves from the outer bed to the inner bed. When the gas:liquid ratio further increases from 200 to 600, the temperature bulge diminishes and the liquid temperature drops below 323 K due to vaporization of water from the liquid to saturate the dry gas stream entering the RPB.

5. MASS TRANSFER STUDIES

Liquid-side mass transfer has been identified as the major resistance to CO_2 chemical absorption in the conventional PB.[40] Much effort has been spent to enhance the liquid-phase mass transfer coefficient by creating turbulence with highly efficient packings even at the cost of larger pressure drops.[41−43] Furthermore, solvents with high viscosity have been considered problematic even though there are many other potential benefits.[44,45] As a process intensification alternative to the conventional PB, the RPB is expected to greatly reduce the liquid-side mass transfer resistance with the rotational gravity and impact solvent selection and process development. This section intends to quantify the resistances from the liquid-phase mass transfer, gas-phase mass transfer, and reaction kinetics using the validated RPB model developed in this work and provide insights into future solvent selection and process development for the RPB.

To determine the contributions of each resistance to CO_2 flux in the RPB, we manually perturb k_L, k_G, and k_j^o by 1% and record the corresponding CO_2 removal efficiency. The reaction rate constants k_j^o for both forward and reverse reactions of carbamate formation and bicarbonate formation are altered simultaneously to maintain the chemical equilibrium. The RPB is modeled isothermally at 323 K when each parameter is perturbed to decouple the temperature effect. The effect of the interfacial area between the gas and liquid is decoupled by assigning a constant packing specific area of 400 m^2/m^3 throughout the RPB. The perturbation step size is assigned as 1%, which is larger than the convergence tolerance but small enough to maintain the local linearity.

Figure 7 shows the contributions of each resistance to the CO_2 removal efficiency at various lean loadings. The liquid flow rate was adjusted at each lean loading to maintain the 90% CO_2 removal efficiency as the flue gas rate is fixed. The liquid:gas ratio increases from 1.4 to 5.6 kg/kg as the lean loading increases from 0 to 0.305 mol of CO_2/mol of MEA. Figure 7 shows that the reaction kinetic resistance plays the dominant role in CO_2 absorption, and the CO_2 removal efficiency is most sensitive to the change in the reaction rate constant compared to the changes in the liquid-side and gas-side mass transfer coefficients. As the lean loading increases, the reaction kinetic resistance becomes more pronounced because of the decreasing free MEA concentration, and the liquid-side mass transfer resistance slightly increases to ~0.20 mol of CO_2/mol of MEA. The gas-side resistance is insignificant in the entire lean loading range.

The RPB sensitivity analysis shows that CO_2 absorption is dominated by the reaction kinetic resistance, while prior work showed that the liquid-side mass transfer coefficient is the controlling factor in the conventional PB.[40] Because k_L is greatly enhanced by the turbulence created by the rotational gravity in RPB, the liquid-side mass transfer resistance becomes much diminished, as supported by the Tung and Mah correlation. The diminished role of the liquid-side mass transfer resistance also suggests that solvent viscosity will have a weaker effect on CO_2 absorption. The analysis guides future solvent development for RPB, and the solvents with fast reaction kinetics should be the focus as the liquid-side mass transfer resistance can be effectively reduced by applying rotational gravity.

https://doi.org/10.1021/acs.iecr.1c04323
Ind. Eng. Chem. Res. 2022, 61, 12142−12152

6. CONCLUSIONS

This study presents a first-principle RPB simulation model for CO_2 absorption using a 30 wt % MEA aqueous solution. By properly accounting for the thermodynamic and transport properties, the solution chemistry, the reaction kinetics, and the RPB hydraulics, the rate-based RPB model rigorously calculates the heat and mass transfer with fast reactions across the gas and liquid films. The model satisfactorily correlates the literature lab-scale data by introducing a correction factor for the effective packing surface area across a wide range of lean loadings from 0 to 0.442 mol of CO_2/mol of MEA under high rotational gravity. This work demonstrates that the RPB can be modeled as a PB if the unique features of RPB are properly taken into consideration. These features include the high liquid-phase mass transfer coefficient k_L represented by the Tung and Mah correlation and the effective packing surface area a_e due to the rotational gravity in the radial direction. Among the liquid-phase hydraulics, only a_e affects the CO_2 removal efficiency, whereas k_L and liquid hold ε_L have little impact on the CO_2 removal efficiency. Among the examined a_e correlations, the Onda correlation with an adjustable parameter to scale the effective packing surface area correlates the CO_2 removal efficiency data better than the Luo12 and Luo17 correlations. The results suggest that reliable a_e correlations are essential for accurately predicting the CO_2 removal efficiency in the RPB. Sensitivity analysis showed that the reaction kinetic resistance dominates the CO_2 absorption over the liquid-side and gas-side mass transfer resistances. The high k_L provided by the RPB diminished the importance of the liquid-side mass transfer. Hence, the solvent selection with the RPB should focus on enhancing the fast reaction kinetics. The rigorous RPB model developed in this work will be foundational to the process simulation and design for the CO_2 chemical absorption processes with RPB.

AUTHOR INFORMATION

Corresponding Author

Chau-Chyun Chen − *Department of Chemical Engineering, Texas Tech University, Lubbock, Texas 79409-3121, United States;* orcid.org/0000-0003-0026-9176; Email: chauchyun.chen@ttu.edu

Authors

Cheng-Hsiu Yu − *Department of Chemical Engineering, Texas Tech University, Lubbock, Texas 79409-3121, United States*

Yu-Jeng Lin − *Department of Chemical Engineering, National Tsing Hua University, Hsinchu 30013, Taiwan*

David Shan-Hill Wong − *Department of Chemical Engineering, National Tsing Hua University, Hsinchu 30013, Taiwan*

Complete contact information is available at: https://pubs.acs.org/10.1021/acs.iecr.1c04323

Notes

This report was prepared as an account of work sponsored by an agency of the United States Government. Neither the United States Government nor any agency thereof, nor any of their employees, makes any warranty, express or implied, or assumes any legal liability or responsibility for the accuracy, completeness, or usefulness of any information, apparatus, product, or process disclosed, or represents that its use would not infringe privately owned rights. Reference herein to any specific commercial product, process, or service by trade name, trademark, manufacturer, or otherwise does not necessarily constitute or imply its endorsement, recommendation, or favoring by the United States Government or any agency thereof. The views and opinions of authors expressed herein do not necessarily state or reflect those of the United States Government or any agency thereof.

The authors declare no competing financial interest.

ACKNOWLEDGMENTS

Funding support is provided by the U.S. Department of Energy under Grant DE-EE0007888. The authors gratefully acknowledge the financial support of the Jack Maddox Distinguished Engineering Chair Professorship in Sustainable Energy sponsored by the JF Maddox Foundation.

NOMENCLATURE

a_i = activity of species i
a_e = effective surface area of packing, m^2/m^3
a_t = specific area of packing, m^2/m^3
c = pore diameter defined in refs 27 and 38, mm; 1.8 for Luo12 correlation, 3.0 for Luo17 correlation
c_p = specific molar heat capacity, J $kmol^{-1}$ K^{-1}
C = CO_2 removal efficiency, %
d = wire mesh diameter defined in refs 27 and 38, mm; 0.35 for Luo12 correlation, 0.4 for Luo17 correlation
d_p = effective diameter of packing, $\frac{6(1-\Phi)}{a_t}$, m
D = diffusivity of species i, m^2/s
$\overline{D}$ = average diffusivity, m^2/s
E_j = activation energy for reaction j, kJ mol^{-1}
g_c = centrifugal acceleration, m/s^2
g_o = characteristic centrifugal acceleration,[21] 100 m^2/s
G = superficial mass flux of gas, kg s^{-1} m^{-2}
h = heat transfer coefficient, W m^{-2} K^{-1}
k = mass transfer coefficient, m/s
k_j = reaction rate constant for reaction j at system temperature T
k_j^o = reaction rate constant for reaction j at reference temperature 298.15 K
$\overline{k}$ = average mass transfer coefficient, m/s
L = superficial mass flux of liquid, kg s^{-1} m^{-2}
N_{exp} = number of experiments
N_r = number of reconciled variables, including both input and measured variables
N_{sets} = number of data sets
Q = volumetric flow rate, m^3/s
r = radius of the packing in the RPB, m
R = gas constant
s_{mr} = standard deviation specified for the reconciled variable
U = liquid flow rate per unit area, m/s
U_o = characteristic flow rate per unit area,[21] 0.01 m/s
X_{mr} = measured value of the reconciled variable
X_r = estimated value of the reconciled variable
z = height of the packing, m

GREEK LETTERS

ε_L = liquid holdup, m^3
λ = thermal conductivity, W m^{-1} K^{-1}
μ = viscosity, kg m^{-1} s^{-1}
ν = kinematic viscosity, m^2/s
ν_o = characteristic kinematic viscosity of liquid,[21] 1.0×10^{-6} m^2/s

https://doi.org/10.1021/acs.iecr.1c04323
Ind. Eng. Chem. Res. 2022, 61, 12142−12152

ρ = density, kg/m^3
$\bar{\rho}$ = molar density, kmol/m^3
σ = surface tension, kg/s^2
σ_c = critical surface tension of the packing, kg/s^2; 0.075 for stainless steel wire mesh[28]
φ = packing characteristics for Luo12 and Luo17 correlations, $\frac{c^2}{(d+c)^2}$
Φ = porosity of the packing, dimensionless
ω = angular speed, rad/s

DIMENSIONLESS GROUPS

$$Fr_L = \frac{L^2 a_t}{\rho_L^2 g_c}$$
$$Fr'_L = \frac{Q_L^2}{r\omega^2(2\pi rz)^2 d_p}$$
$$Gr_L = \frac{d_p^3 g_c \rho_L^2}{\mu_L^2}$$
$$Re_L = \frac{L}{a_t \mu_L}$$
$$Re'_L = \frac{Q_L d_p}{(2\pi rz)\upsilon_L}$$
$$Re_G = \frac{G}{a_t \mu_G}$$
$$Re'_G = \frac{Q_G d_p}{(2\pi rz)\upsilon_G}$$
$$Sc_L = \frac{\mu_L}{\rho_L D_L}$$
$$Sc_G = \frac{\mu_G}{\rho_G D_G}$$
$$We_L = \frac{L^2}{\rho_L \sigma_L a_t}$$
$$We'_L = \frac{Q_L^2 \rho_L d_p}{(2\pi rz)^2 \sigma_L}$$

SUPERSCRIPTS AND SUBSCRIPTS

cal = calculated
exp = experimental
f = forward reaction
G = gas phase
L = liquid phase
r = reverse reaction

REFERENCES

(1) Rochelle, G. T. Amine scrubbing for CO_2 capture. *Science* **2009**, *325*, 1652−1654.
(2) Yu, C. H.; Huang, C. H.; Tan, C. S. A review of CO_2 capture by absorption and adsorption. *Aerosol Air Qual. Res.* **2012**, *12*, 745−769.
(3) Jassim, M. S.; Rochelle, G. T.; Eimer, D.; Ramshaw, C. Carbon dioxide absorption and desorption in aqueous monoethanolamine solutions in a rotating packed bed. *Ind. Eng. Chem. Res.* **2007**, *46*, 2823−2833.
(4) Yu, C. H.; Cheng, H. H.; Tan, C. S. CO_2 capture by alkanolamine solutions containing diethylenetriamine and piperazine in a rotating packed bed. *Int. J. Greenh. Con.* **2012**, *9*, 136−147.
(5) Yu, C. H.; Wu, T. W.; Tan, C. S. CO_2 capture by piperazine mixed with non-aqueous solvent diethylene glycol in a rotating packed bed. *Int. J. Greenh. Con.* **2013**, *19*, 503−509.
(6) Thiels, M.; Wong, D. S. H.; Yu, C. H.; Kang, J. L.; Jang, S. S.; Tan, C. S. Modeling and design of carbon dioxide absorption in rotating packed bed and packed column. *IFAC-PapersOnLine* **2016**, *49*, 895−900.
(7) Yu, C. H.; Chen, M. T.; Chen, H.; Tan, C. S. Effects of process configurations for combination of rotating packed bed and packed bed on CO_2 capture. *Appl. Energy* **2016**, *175*, 269−276.
(8) Chamchan, N.; Chang, J. Y.; Hsu, H. C.; Kang, J. L.; Wong, D. S. H.; Jang, S. S.; Shen, J. F. Comparison of rotating packed bed and packed bed absorber in pilot plant and model simulation for CO_2 capture. *J. Taiwan Inst. Chem. Eng.* **2017**, *73*, 20−26.
(9) Wang, Y. M.; Chen, Y. S. Capture of CO_2 by highly concentrated alkanolamine solutions in a rotating packed bed. *Environ. Prog. Sustainable Energy* **2019**, *38*, e13263.
(10) Xie, C. X.; Dong, Y. N.; Zhang, L. L.; Chu, G. W.; Luo, Y.; Sun, B. C.; Zeng, X. F.; Chen, J. F. Low-concentration CO_2 capture from natural gas power plants using a rotating packed bed reactor. *Energy Fuel* **2019**, *33*, 1713−1721.
(11) Kang, J. L.; Sun, K.; Wong, D. S. H.; Jang, S. S.; Tan, C. S. Modeling studies on absorption of CO_2 by monoethanolamine in rotating packed bed. *Int. J. of Greenh. Gas Con.* **2014**, *25*, 141−150.
(12) Joel, A. S.; Wang, M.; Ramshaw, C.; Oko, E. Process analysis of intensified absorber for post-combustion CO_2 capture through modelling and simulation. *Int. J. of Greenh. Gas Con.* **2014**, *21*, 91−100.
(13) Joel, A. S.; Wang, M.; Ramshaw, C. Modelling and simulation of intensified absorber for post-combustion CO_2 capture using different mass transfer correlations. *Appl. Therm. Eng.* **2015**, *74*, 47−53.
(14) Oko, E.; Ramshaw, C.; Wang, M. Study of intercooling for rotating packed bed absorbers in intensified solvent-based CO_2 capture process. *Appl. Energy* **2018**, *223*, 302−316.
(15) Borhani, T. N.; Oko, E.; Wang, M. Process modelling and analysis of intensified CO_2 capture using monoethanolamine (MEA) in rotating packed bed absorber. *J. Clean. Prod.* **2018**, *204*, 1124−1142.
(16) Hikita, H.; Asai, S.; Ishikawa, H.; Honda, M. The kinetics of reactions of carbon dioxide with monoethanolamine, diethanolamine and triethanolamine by a rapid mixing method. *Chem. Eng. J.* **1977**, *13*, 7−12.
(17) Onda, K.; Takeuchi, H.; Okumoto, Y. Mass transfer coefficients between gas and liquid phases in packed columns. *J. Chem. Eng. Jpn.* **1968**, *1*, 56−62.
(18) Tung, H.-H.; Mah, R. S. Modeling liquid mass transfer in HIGEE separation process. *Chem. Eng. Commun.* **1985**, *39*, 147−153.
(19) Aboudheir, A.; Tontiwachwuthikul, P.; Chakma, A.; Idem, R. Kinetics of the reactive absorption of carbon dioxide in high CO_2-loaded, concentrated aqueous monoethanolamine solutions. *Chem. Eng. Sci.* **2003**, *58*, 5195−5210.
(20) Austgen, D. M.; Rochelle, G. T.; Peng, X.; Chen, C.-C. Model of vapor-liquid equilibria for aqueous acid gas-alkanolamine systems using the electrolyte-NRTL equation. *Ind. Eng. Chem. Res.* **1989**, *28*, 1060−1073.
(21) Burns, J.; Jamil, J.; Ramshaw, C. Process intensification: operating characteristics of rotating packed beds−determination of liquid hold-up for a high-voidage structured packing. *Chem. Eng. Sci.* **2000**, *55*, 2401−2415.
(22) Billet, R.; Schultes, M. Predicting mass transfer in packed columns. *Chem. Eng. Technol.* **1993**, *16*, 1−9.
(23) Chen, Y. S. Correlations of mass transfer coefficients in a rotating packed bed. *Ind. Eng. Chem. Res.* **2011**, *50*, 1778−1785.
(24) Luo, X.; Hartono, A.; Hussain, S.; Svendsen, F. H. Mass transfer and kinetics of carbon dioxide absorption into loaded aqueous monoethanolamine solutions. *Chem. Eng. Sci.* **2015**, *123*, 57−69.
(25) Wellek, R. M.; Brunson, R. J.; Law, F. H. Enhancement factors for gas-absorption with second-order irreversible chemical reaction. *Can. J. Chem. Eng.* **1978**, *56*, 181−186.
(26) Aspen Technology Inc. Aspen physical properties system: physical property methods. 2010.
(27) Luo, Y.; Chu, G. W.; Zou, H. K.; Zhao, Z. Q.; Dudukovic, M. P.; Chen, J. F. Gas-liquid effective interfacial area in a rotating packed bed. *Ind. Eng. Chem. Res.* **2012**, *51*, 16320−16325.
(28) Chen, Y. S.; Lin, F. Y.; Lin, C. C.; Tai, C. Y. D.; Liu, H. S. Packing characteristics for mass transfer in a rotating packed bed. *Ind. Eng. Chem. Res.* **2006**, *45*, 6846−6853.

https://doi.org/10.1021/acs.iecr.1c04323
Ind. Eng. Chem. Res. 2022, 61, 12142−12152

(29) Zhang, Y.; Que, H.; Chen, C.-C. Thermodynamic modeling for CO_2 absorption in aqueous MEA solution with electrolyte NRTL model. *Fluid Phase Equilib.* **2011**, *311*, 67−75.
(30) Plaza, J. M. Modeling of carbon dioxide absorption using aqueous monoethanolamine, piperazine and promoted potassium carbonate. Ph.D. Dissertation, The University of Texas at Austin, Austin, TX, 2012.
(31) *Aspen Plus*, ver. 10; Aspen Technology Inc.: Burlington, MA, 2017.
(32) Aspen Technology Inc. Rate-based model of the CO_2 capture process by MEA using Aspen Plus. 2008.
(33) Zhang, Y.; Chen, H.; Chen, C.-C.; Plaza, J. M.; Dugas, R.; Rochelle, G. T. Rate-based process modeling study of CO_2 capture with aqueous monoethanolamine solution. *Ind. Eng. Chem. Res.* **2009**, *48*, 9233−9246.
(34) Zhang, Y.; Chen, C.-C. Modeling CO_2 absorption and desorption by aqueous monoethanolamine solution with Aspen rate-based model. *Energy Procedia* **2013**, *37*, 1584−1596.
(35) Gross, J.; Sadowski, G. Perturbed-Chain SAFT: An equation of state based on a perturbation theory for chain molecules. *Ind. Eng. Chem. Res.* **2001**, *40*, 1244−1260.
(36) Weiland, R. H.; Dingman, J. C.; Cronin, D. B.; Browning, G. J. Density and viscosity of some partially carbonated aqueous alkanolamine solutions and their Blends. *J. Chem. Eng. Data* **1998**, *43*, 378−382.
(37) Taylor, R.; Krishna, R. *Multicomponent mass transfer*; Wiley: New York, 1993.
(38) Luo, Y.; Luo, J. Z.; Chu, G. W.; Zhao, Z. Q.; Arowo, M.; Chen, J. F. Investigation of effective interfacial area in a rotating packed bed with structured stainless steel wire mesh packing. *Chem. Eng. Sci.* **2017**, *170*, 347−354.
(39) Chen, C. H. Applications of concentrated alkanolamine solutions on CO_2 absorption in rotating packed bed. Master's Thesis, National Tsing Hua University, Hsinchu, Taiwan, 2012 (https://hdl.handle.net/11296/uf5z66).
(40) Sachde, D. J. Absorber performance and configurations for CO_2 capture using aqueous piperazine. Ph.D. Dissertation, The University of Texas at Austin, Austin, TX, 2016.
(41) Tsai, R. E. Mass transfer area of structured packing. Ph.D. Dissertation, The University of Texas at Austin, Austin, TX, 2010.
(42) Tan, L. S.; Shariff, A. M.; Lau, K. K.; Bustam, M. A. Factors affecting CO_2 absorption efficiency in packed column: A review. *J. Ind. Eng. Chem.* **2012**, *18*, 1874−1883.
(43) Wang, C.; Perry, M.; Seibert, F.; Rochelle, G. Packing characterization for post combustion CO_2 capture: mass transfer model development. *Energy Procedia* **2014**, *63*, 1727−1744.
(44) Ramdin, M.; de Loos, T. W.; Vlugt, T. J. H. State-of-the-Art of CO_2 capture with ionic liquids. *Ind. Eng. Chem. Res.* **2012**, *51*, 8149−8177.
(45) Krupiczka, R.; Rotkegel, A.; Ziobrowski, Z. Comparative study of CO_2 absorption in packed column using imidazolium based ionic liquids and MEA solution. *Sep. Purif. Technol.* **2015**, *149*, 228−236.

https://doi.org/10.1021/acs.iecr.1c04323
Ind. Eng. Chem. Res. 2022, 61, 12142−12152